International Journal of Microwave and Wireless Technologies

cambridge.org/mrf

High-gain circularly polarized Fabry–Perot resonator antenna based on advanced polarization conversion metasurface

Xin He, Wenhua Qin, Kaize Wang and Juan Xu

Cyberspace Security Academy, Qufu Normal University, Qufu, China

Research Paper

Cite this article: He X, Qin W, Wang K, Xu J (2024) High-gain circularly polarized Fabry–Perot resonator antenna based on advanced polarization conversion metasurface. *International Journal of Microwave and Wireless Technologies* **16**(10), 1705–1712. https://doi.org/10.1017/S175907872500011X

Received: 7 July 2024
Revised: 14 January 2025
Accepted: 18 January 2025

Keywords:
circular polarized; Fabry-Perot resonator antenna; high gain; polarization conversion

Corresponding author: Juan Xu;
Email: xujuan125@163.com

Abstract

In this paper, a novel polarization conversion metasurface (PCM) is proposed. Compared with the conventional receiver-transmitter metasurface units, two metallized via holes are set up to correct the current. It can achieve better polarization conversion from linear to circular and maintain a high reflectivity performance. A patch antenna with an L-probe feed is used as a feeder. The circularly polarized Fabry–Perot resonator antenna (CP-FPRA) consists of the PCM with a 5 × 5 array and a feeder. The measurements indicate a 3 dB axial ratio (AR) bandwidth of 8.6% (22.3–24.3 GHz). And it achieves a maximum gain of 14.2 dBic at 24 GHz, compared to the feed antenna has a gain enhancement of 5.5 dBi (from 8.7 dBi to 14.2 dBic). The proposed CP-FPRA has high gain, a wide AR, and a relatively low profile, providing ideas for subsequent antenna designs.

Introduction

Nowadays, antennas are rapidly developing, the characteristics of antennas, such as high gain, circularly polarization (CP), and simple structure are getting more and more attention. Due to the Fabry–Perot resonator antenna (FPRA) simple structure, easy integration, and high gain, it is a nice method for design [1–10]. Today, there are several methods to realize the circularly polarized FPRA (CP-FPRA): CP feed antenna and polarization conversion metasurface (PCM).

In papers [1, 2], proposed sequential feed antenna arrays are used as CP feed antennas for FPRA. Both antennas achieve good CP radiation but have complex feed networks. The feed antennas are reconfigurable CP antennas [3, 4]. They can operate in different polarization states, but they have no advantages in processing and maintenance. Papers [5–10] show a suitable PCM to achieve CP radiation. Two orthogonal linear polarization (LP) waves present a 90° transmission phase difference to form a CP wave. For CP-FPRA, the PCM is usually a metasurface with reflective and transmissive properties. The conventional receiver-transmitter (RT) metasurfaces have a metallized plane to separate the lower and upper layers of receiver and transmitter patches [11, 12]. And incident waves by metallized through-holes achieve coupling [13–15]. When receives the LP and radiates the CP, the PCM shows a performance of polarization conversion. Therefore, it is feasible to design the CP-FPRA with a PCM based on RT unit.

In this paper, a novel RT-based PCM unit with two metallized via-holes is proposed for the design of CP-FPRA. Metallized via-holes are used to connect the receiver and transmitter of the PCM unit and correct the current to achieve LP to CP conversion. Meanwhile, it maintains high reflectivity to ensure a high gain of the CP-FPRA. PCM and the feed antenna are combined to form the CP-FPRA. The proposed CP-FPRA achieves high gain and wide axial ratio (AR). The 3 dB AR bandwidth of 8.6% (22.3–24.3 GHz) and a peek gain reaches 14.2 dBic at 24 GHz.

Antenna design and analysis

CP-FPRA configuration

The configuration of the proposed CP FPRA is shown in Figure 1. The antenna consists of a PCM and a feed antenna. The h represents the distance between PCM and the feed antenna, it determines the final profile of the antenna. The LP waves are radiated from the feeder and reflected in the cavity (formed by the PCM and the ground plane). At the same time, the LP resonance is realized in the cavity, and the PCM convert the LP waves in the cavity into CP waves. The resonance generation of CP-FPRA and the conversion of LP to CP are spatially separated.

Operating principles

CP-FPRA can work when Equation (1) is satisfied, h (distance between the PCM and the feed antenna) determines the final profile of the antenna [16].

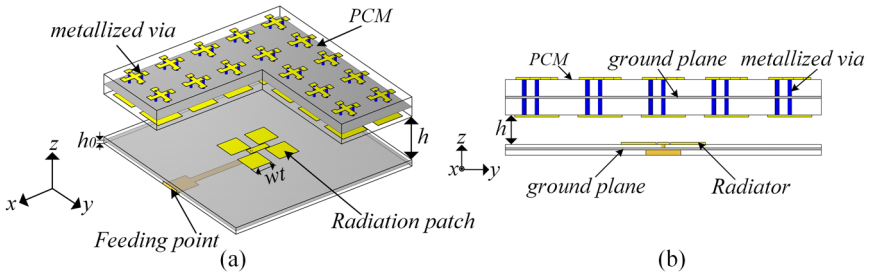

Figure 1. Geometry of the proposed CP-FP antenna. (a) CP-FPRA oversize. (b) CP-FPRA side view.

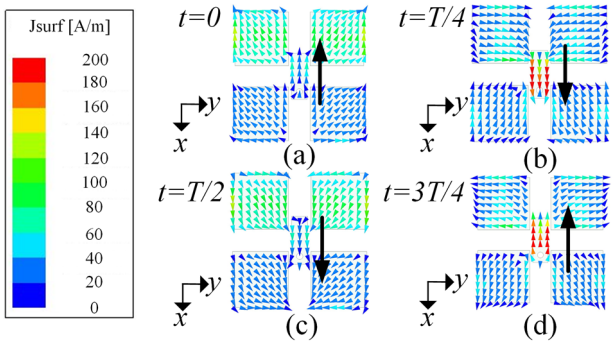

Figure 2. The feed antenna surface current distribution of the top patch at 24 GHz. (a) $t = 0$, (b) $t = T/4$, (c) $t = T/2$, (d) $t = 3T/4$.

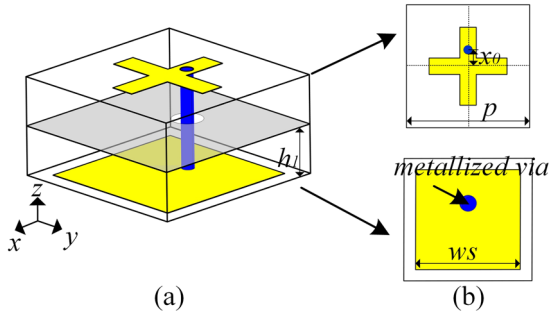

Figure 3. Configuration of the original unit cell. (a) 3D sketch. (b) Detailed structure.

$$\varphi_S - \varphi_D - \frac{4\pi h}{\lambda_0} = 2N\pi, N = 0, \pm 1, \pm 2, \ldots \quad (1)$$

where $\lambda_0 = \frac{c}{f_0}$, $f_0$is the operating frequency, $\varphi_S$is the reflection phases of the PCM, and $\varphi_D$is the reflection phases of ground plane.

According to the full-wave analysis and measurement verification, the calculated relationship between the directivity D of CP-FPRA and the reflection coefficient $\Gamma$of PCM can be obtained as follows (Equation (2)) [17]:

$$D = 10\log_{10}\frac{1 + |\Gamma|}{1 - |\Gamma|} \quad (2)$$

It found the directivity D of the CP-FPRA is higher when the PCM reflection coefficient $\Gamma$is larger, thus enhancing the antenna gain. Therefore, the high reflectivity of the PCM ensures a high gain of the CP-FPRA. In addition, the following conditions are required to realize the polarization conversion: the magnitude of the transmission coefficients is $T_{xx} = T_{yx}$and the transmission phase difference is $(\varphi T_{xx} - \varphi T_{yx}) = 90^\circ$ [8].

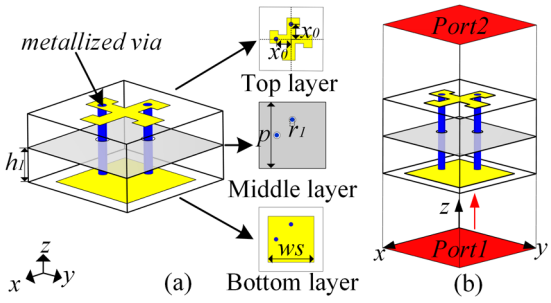

Figure 4. Configuration of the proposed polarization conversion unit. (a) Detailed structure. (b) Simulation model of the unit.

Design and analysis of feed antenna

A CP-FPRA with good performance requires a good feed antenna. The feed antenna as shown in Figure 1(a), the two layer dielectric substrates are made of Rogers 5880 ($\varepsilon_r = 2.2$, $\tan\delta = 0.0009$), the thickness $h_0 = 0.508$ mm. The top layer consists of four identical square patches as the radiation patch, the metallized plane is printed between the two dielectric substrates. And the bottom layer is fed using a microstrip line and transmits energy through an L-shaped probe.

Figure 2 shows the simulated current distribution of the feed antenna on one T (T is the period of the excitation signal) at 24 GHz. At $t = 0$, the current is mainly concentrated on the square patches, and the current flows along the negative x-axis. At $t = T/4$, the current is mainly concentrated at the middle rectangular patch, and the current direction is along the positive x-axis. When $t = T/2$ and $3T/4$, the current distribution is similar to at $t = 0$ and $T/4$, but has the opposite direction. Therefore, the feed antenna periodically radiates x-polarization.

Design process of PCM

Development of PCM unit

Figure 3 shows configuration of the original unit cell. The period of unit $p = 6$ mm ($0.48\lambda_0$), it has two same substrates ("Rogers 5880," $\varepsilon_r = 2.2$, $h_1 = 1.57$ mm) and three layers of metal patches. The top layer is a cross-shaped structure (as the transmitter), the middle layer is a metallized plane, and the bottom layer is a square patch ($w_s = 4.9$ mm), acts as the receiver. A metallized via is set in the x-axis offset from the origin $x_0 (x_0 = 0.8$ mm).

Figure 4 is developed from Figure 3 has two differences. First, a rectangle is sequentially added at the end of the cross-patch on the upper layer. This addition can increase the electrical length of the patch, improve the transmission performance of the unit,

https://doi.org/10.1017/S1759078725000011X Published online by Cambridge University Press

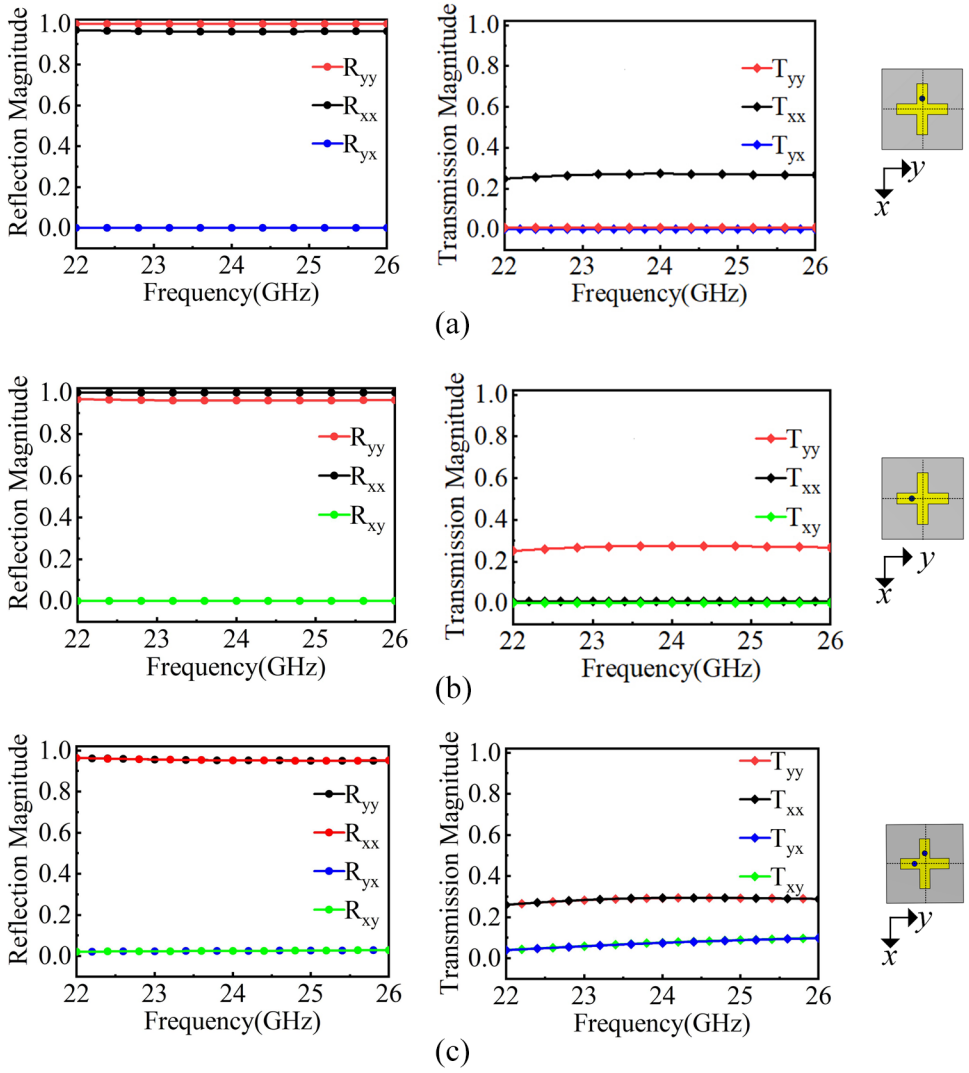

Figure 5. (a) Simulated *S* parameters of the original unit cell with metallized via in the *x*-axis. (b) Simulated *S* parameters of the original unit cell with metallized via in the *y*-axis. (c) Simulated *S* parameters of the original unit cell with metallized vias in the *x*-axis and *y*-axis.

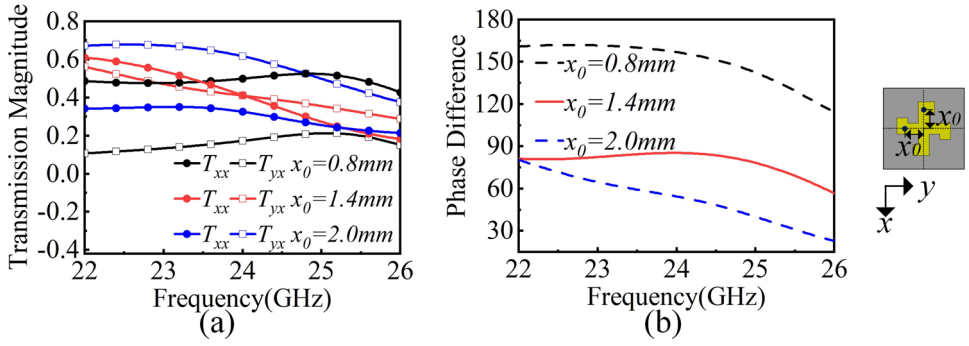

Figure 6. Effect of $x_0$on the *S* parameters of the proposed polarization conversion unit cell. (a) Transmission coefficients. (b) Phase difference.

and ensure the stability at a certain angle (maintaining consistent performance when the electromagnetic wave is incident at various angles). Second, added a metallized via in the *y*-axis to correct the current and achieve better polarization conversion. Figure 4(b) shows the simulation model of the proposed PCM unit in the High Frequency Structure Simulator (HFSS). Port 1 and Port 2 are set Floquet ports. And Port 1 is the excitation port.

Figure 5 provides data to support the above. Figure 5(a) shows simulated *S* parameters of the original unit cell with metallized via in the *x*-axis. The reflectivity of co-polarization reaches 0.98,

https://doi.org/10.1017/S1759078725000011X Published online by Cambridge University Press

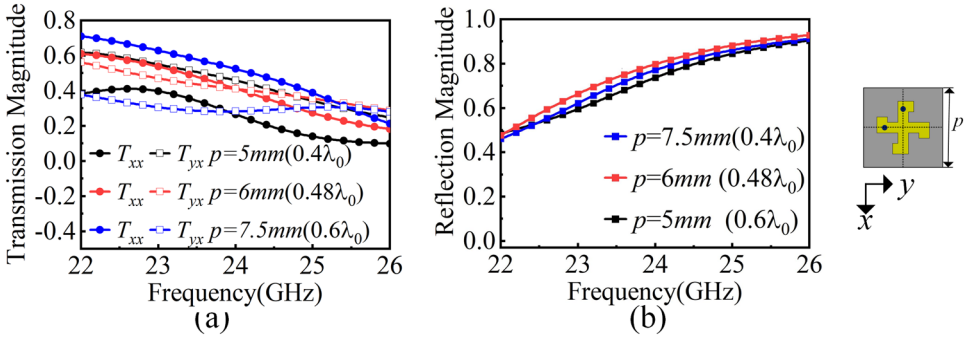

Figure 7. Effect of p on the S parameters of the proposed polarization conversion unit cell. (a) Transmission coefficients. (b) Reflection coefficients.

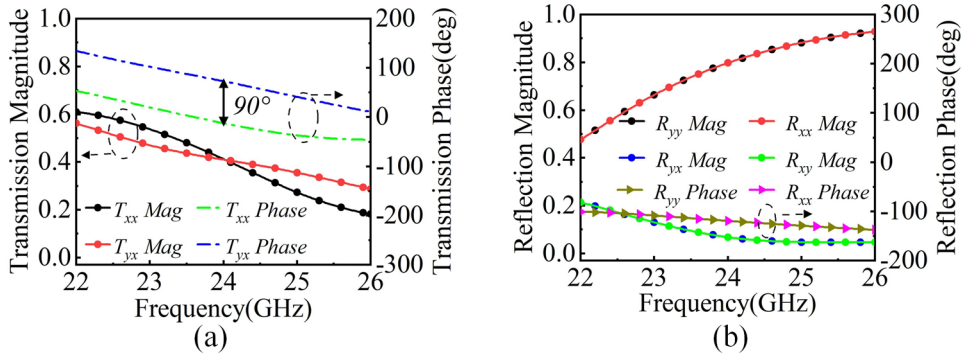

Figure 8. Simulated S parameters of the proposed unit cell versus frequency. (a) Transmission coefficients. (b) Reflection coefficients.

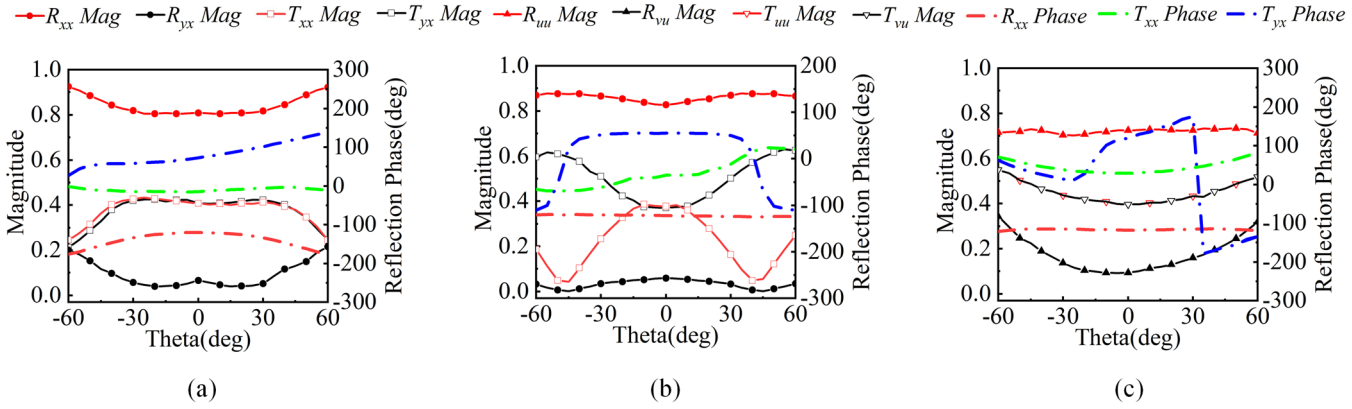

Figure 9. Simulated S parameters of the proposed unit cell versus the angle. (a) 24 GHz in the *xoz* plane. (b) 24 GHz in the *yoz* plane. (c) 24 GHz in the phi = 45° plane.

but the reflectivity of cross-polarization is almost 0. The $T_{xx}$is keep above 0.2, while the $T_{yy}$and $T_{yx}$are almost 0. So, the unit can transmit a part of the x-polarization and prevent the y-polarization. And it cannot realize the polarization conversion. Correspondingly, Figure 5(b) shows the metallized via in the y-axis. The unit can pass through a part of the y-polarization and prevent the x-polarization, and still not have the polarization conversion function.

Figure 5(c) illustrates the reflection and transmission of the unit with two equally spaced metallized vias. The second metallized via unaffected the reflection performance, and the co-polarization transmission of the unit. But can improve the transmission of cross-polarization of the unit. So, a suitable $x_0$can achieve T_{xx}= T_{yx}.

Figure 6 shows the variation of the transmission coefficients with the position x_0. When x_0= 1.4 mm, the transmission coefficient $T_{xx}$of the proposed unit is equal to T_{yx}at 24 GHz. And the transmission performance is improved compared with original cell. The transmission phase difference decreases as the $x_0$increases. When x_0= 1.4 mm, the phase difference is 90°, at 24 GHz. This satisfies the conditions for a polarization conversion.

Figure 7 shows the variation of the transmission and reflection coefficients with the p (period of unit). When p = 6 mm (0.48λ_0), the transmission coefficient T_{xx}= T_{yx}, at 24 GHz. And the reflection magnitude first increases and then decreases, as the value of p increases. From Equation (2), a larger the reflection magnitude results in a higher antenna gain. So,

https://doi.org/10.1017/S1759078725000011X Published online by Cambridge University Press

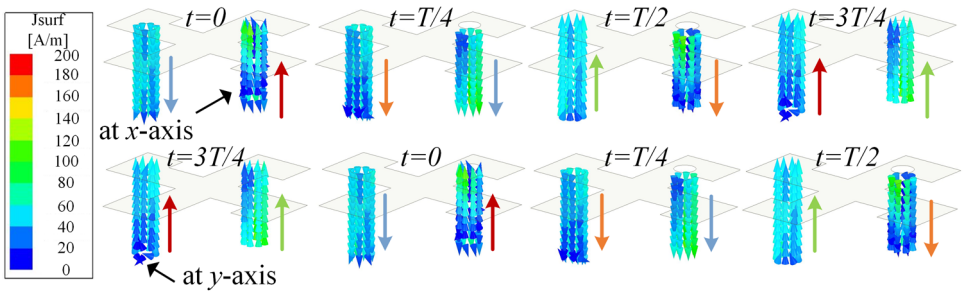

Figure 10. The current distribution of metallized via in the proposed polarization conversion unit.

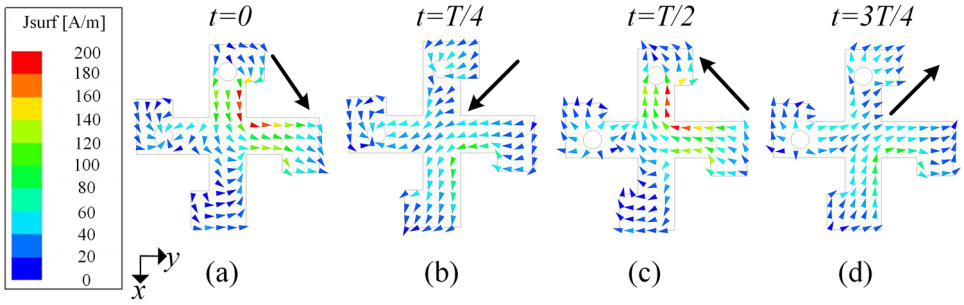

Figure 11. The current distribution of the upper patch of the proposed polarization conversion unit. (a) $t = 0$, (b) $t = T/2$, (c) $t = 3T/4$, (d) and $t = T$.

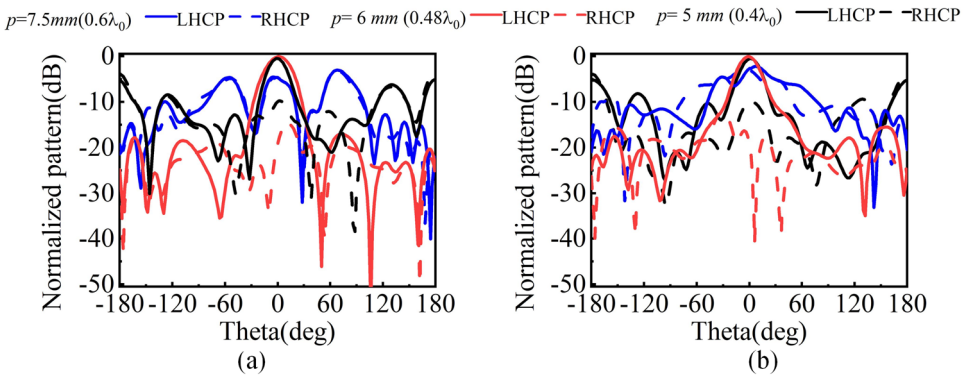

Figure 12. Simulated normalized radiation patterns of the antenna with change *p*. (a) *xoz* plane at 24 GHz. (b) *yoz* plane at 24 GHz.

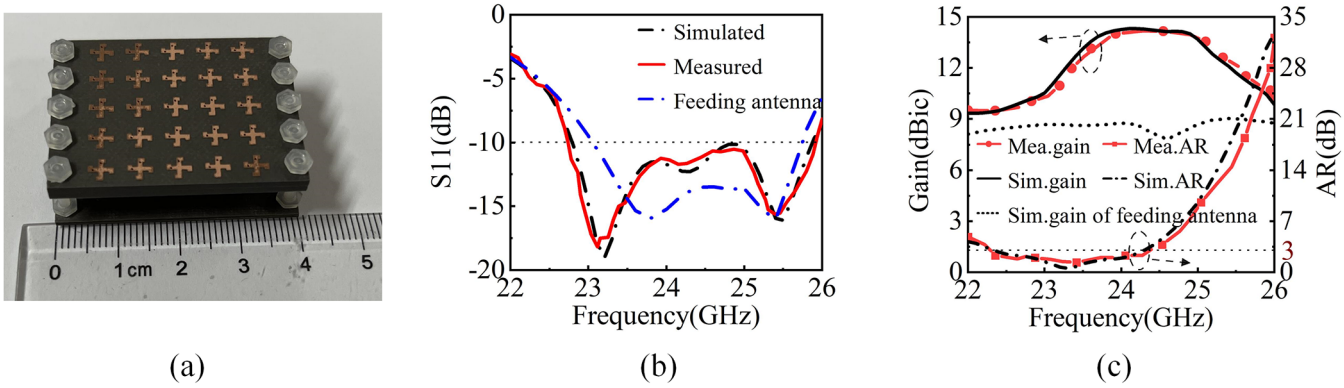

Figure 13. (a) Photographs of fabricated antenna. (b) S_{11} of simulated and measured results. (c) AR and gain of simulated and measured results.

https://doi.org/10.1017/S1759078725000011X Published online by Cambridge University Press

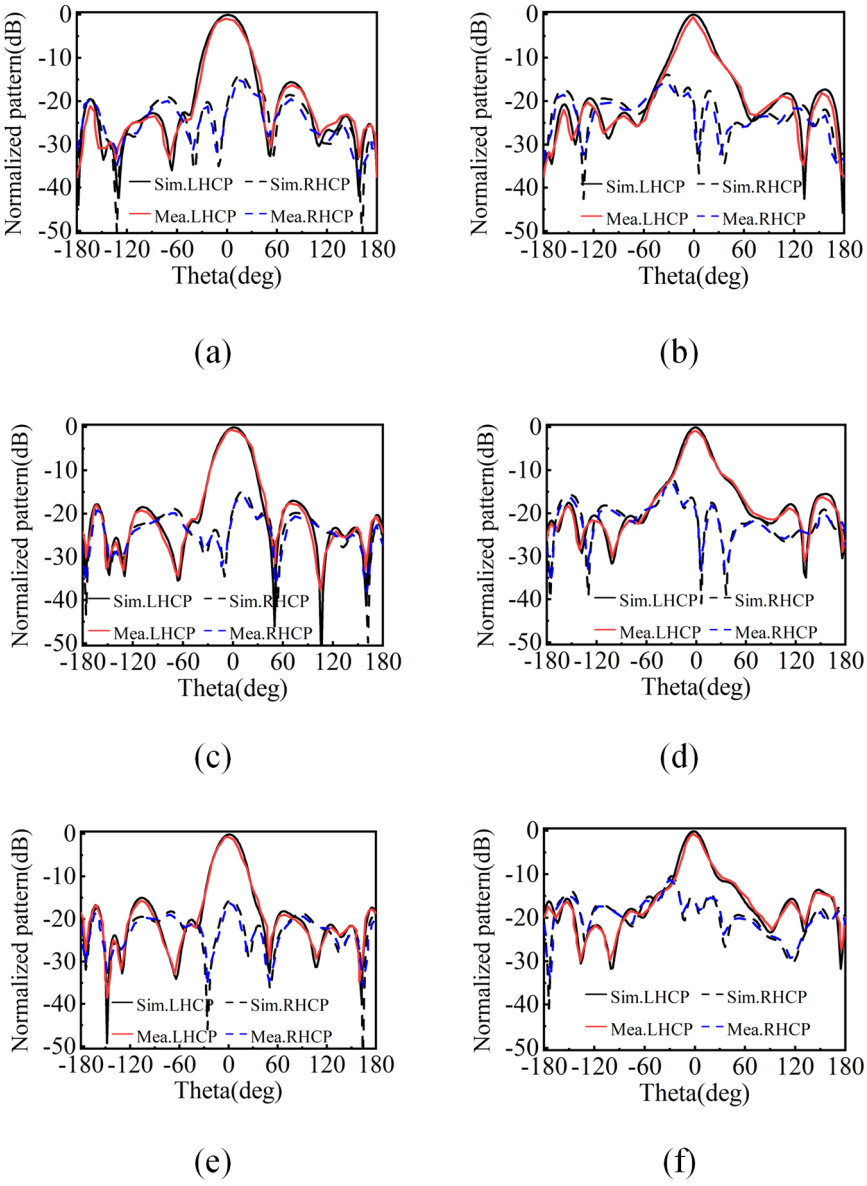

Figure 14. Simulated and measured normalized radiation patterns of the antenna. (a) *xoz* plane at 23.7 GHz. (b) *yoz* plane at 23.7 GHz. (c) *xoz* plane at 24 GHz. (d) *yoz* plane at 24 GHz. (e) *xoz* plane at 24.3 GHz. (f) *yoz* plane at 24.3 GHz.

$p = 6$ mm ($0.48\lambda_0$) was chosen, it is good for enhancing antenna radiation.

Properties of PCM unit

Figure 8 presents the transmission and reflection characteristics of the optimized PCM unit with normal incidence. The transmission coefficients $T_{xx} = T_{yx}$ and has a phase difference of 90° at 24 GHz. The reflection phase of the unit is −120° at 24 GHz. After optimization with HFSS, h is set to 6.9 mm. It is determined the PCM consists of 5 × 5 units with dimensions of 30×30 mm^2.

To demonstrate the angular stability of the proposed unit. Figure 9 plots the S parameters of the unit cell versus the incident angle at 24 GHz. The *xoz, yoz*, and phi = 45°planes are simulated. When the incident angle is less than 15°, horizontal polarization transmission coefficient is equal to vertical polarization transmission coefficient in any plane. Meanwhile a phase difference between 90° ± 15°, it can achieve polarization conversion while maintaining a high co-polarization reflectivity.

Current analysis of PCM

To further explore the polarization conversion function of the proposed unit, the current distribution of the proposed units at 24 GHz is analyzed. Since the feed antenna radiates x-polarization, each unit is excited by x-polarized waves.

Figure 10 illustrates the current distribution of metallized vias in the proposed unit at 24 GHz. When $t = 0$, the current of metallized via-holes in the x-direction is upward, and $t = 3\ T/4$, the current of metallized via-holes in the y-direction flows upward. Correspondingly, at $t = T/4$, the current of metallized via-holes in the x-direction is the same as the current of metallized via-holes in the y-direction at $t = 0$. So, compared with the current of metallized via-holes in the x-direction, the current of metallized

https://doi.org/10.1017/S175907872500011X Published online by Cambridge University Press

Table 1. Comparison of the proposed antenna with previously reported antennas

Ref	PM	BW (GHz)	PG	GE (dBi)	AR (GHz)	Size (λ_0)	NME
[4]	L	6.15–6.6 (7.1%)	6.6 dB	4.1	–	1.47 × 1.47	5 × 5
[8]	C	9.78–10.26 (4.8%)	17.8 dBi	–	9.7–10.35 (6.5%)	3 × 3	9 × 9
[18]	C	15.24–15.34 (0.65%)	14.2 dBi	–	15.24–15.34 (1.2%)	5 × 5	20 × 20
[19]	C	9.86–10.14 (2.8%)	13.4 dBi	–	9.75–10.25 (5%)	2.6 × 2.6	10 × 10
[20]	L	2.32–2.40 (3.4%)	11.5 dB	5.5	–	1.43 × 1.43	6 × 6
This work	C	22.83–25.70 (12 %)	14.2 dBi	5.5	22.3–24.3 (8.6%)	2.4 × 2.4	5 × 5

Abbreviations: L: linear, C: circular, PM: polarization mode, BW: bandwidth, PG: peak gain, GE: gain enhancement, NME: number of metasurface elements.

via-holes in the y-direction is delayed by $T/4$ time. In other word, the unit has a 90° phase difference.

Figure 11 shows the current distribution of the upper radiation patch at 24 GHz. The current alternates in quarter cycles with clockwise rotation, enabling Left-handed circular polarization (LHCP) radiation. Therefore, the proposed unit has a polarization conversion function.

Array analysis and experimental results

To further explain the impact of grating lobes on antenna radiation. Figure 12 shows the effect of PCM with different values of p on the normalized radiation performance of CP-FPRA. When $p = 5$ mm ($0.4\lambda_0$) and $p = 7.5$ mm ($0.6\lambda_0$), the levels of cross-polarization are excessively high, and the effect of the gating lobes is noticeable. $p = 6$ mm ($0.48\lambda_0$) significantly enhances radiation performance and effectively suppresses the effects of gating lobes.

Figure 13(a) shows a fabricated prototype of the proposed CP-FPRA. Figure 13(b) shows the simulated and measured results of $|S_{11}|$. The simulated $|S_{11}| < -10$ dB of CP-FPRA is 12.3% (22.8–25.8 GHz), the measured result reaches 12% (22.83–25.7 GHz). The simulated $|S_{11}| < -10$ dB of feed antenna is 9.4% (23.3–25.6 GHz). It found the antenna impedance bandwidth is increased by adding PCM. Figure 13(c) plots the gain of CP-FPRA and the feed antenna, AR of CP-FPRA. The top dotted arrow points to the gain and the bottom dotted arrow points to the AR. The antenna achieves peak gain at 24 GHz with a simulated result of 14.41 dBic and a measured result of 14.2 dBic. A gain enhancement of 5.5 dBi (from 8.7 dBi to 14.2 dBic) is achieved by adding the PCM. The simulated 3 dB AR band of the CP-FPRA is 9% (22.2–24.3 GHz), and the measured result is 8.6% (22.3–24.3 GHz). The difference between the test results and the simulated results may be in antenna assembly and testing procedures.

Figure 14 shows the simulated and measured normalized radiation patterns of the CP-FPRA. At 24 GHz, the cross-polarization levels are lower than −34 dB, shows low side lobe (<−18 dB), and radiates LHCP. The 3 dB half-power beamwidth extends up to ±11° in the *xoz* and *yoz* planes. At 24.3 GHz (the frequency band edge), the cross-polarization levels are higher. However, the main beam is still LHCP. The measured and simulated results almost match.

Table 1 presents a comparison between the proposed antenna and other antennas in previous articles. Compared with Refs [8, 18] and [19] its AR bandwidth and array size have a significant advantage. Compared with the Refs [4] and [20], the antenna achieves the conversion of LP to CP, while significantly improving the gain. The proposed CP-FPRA is capable of CP radiation by utilizing a PCM with a feed antenna positioned normally, while enhancing the feed antenna gain with a compact profile.

Conclusion

In this paper, a novel PCM unit is proposed. The metallized vias can achieve polarization conversion and maintain stable transmission and reflection coefficients. The CP-FPRA is obtained by combining this PCM and the feed antenna. The proposed CP-FPRA has high gain, wide AR, and a relatively low profile. It achieves a peak gain of 14.2 dBic at 24 GHz, compared to the feed antenna has a gain enhancement of 5.5 dBi (from 8.7 dBi to 14.2 dBic). The bandwidth of AR < 3 dB is 8.6% (22.3–24.3 GHz). The proposed design is a new method for achieving antenna high-gain and CP radiation.

Funding statement. This work was supported in part by the Shandong Natural Science Foundation of ZR2023MF038 and the National Natural Science Foundation of China (61701278).

Competing interests. The author declares that there is no conflict of interest regarding the publication of this paper.

References

1. **Li K, Liu Y, Jia Y and Guo YJ** (2017) A circularly polarized high-gain antenna with low RCS over a wideband using chessboard polarization conversion metasurfaces. *IEEE Transactions on Antennas and Propagation* **65**(8), 4288–4292. doi:10.1109/TAP.2017.2710231
2. **Zarbakhs S, Akbari M, Samadi F and Sebak A-R** (2019) Broadband and high-gain circularly-polarized antenna with low RCS. *IEEE Transactions on Antennas and Propagation* **67**(1), 16–23. doi:10.1109/TAP.2018.2876234
3. **Ji L-Y, Qin P-Y, Guo YJ, Ding C, Fu G and Gong S-X** (2016) A wideband polarization reconfigurable antenna with partially reflective surface. *IEEE Transactions on Antennas and Propagation* **64**(10), 4534–4538. doi:10.1109/TAP.2016.2593716
4. **Zhang J, Liu Y, Jia Y and Zhang R** (2022) High-gain Fabry–Pérot antenna with reconfigurable scattering patterns based on varactor diodes. *IEEE Transactions on Antennas and Propagation* **70**(2), 922–930. doi:10.1109/TAP.2021.3111234
5. **Orr R, Goussetis G and Fusco V** (2014) Design method for circularly polarized Fabry–Perot cavity antennas. *IEEE Transactions on Antennas and Propagation* **62**(1), 19–26. doi:10.1109/TAP.2013.2286839
6. **Liu Z-G, Cao Z-X and Wu L-N** (2016) Compact low-profile circularly polarized Fabry–Perot resonator antenna fed by linearly polarized microstrip patch. *IEEE Antennas and Wireless Propagation Letters* **15**, 524–527. doi:10.1109/LAWP.2015.2456886
7. **Sheersha JA, Nasimuddin N and Alphones A** (2019) A high gain wideband circularly polarized antenna with asymmetric metasurface. *International Journal of RF and Microwave Computer-Aided Engineering* **29**(7), Art. no e21740. doi:10.1002/mmce.21740
8. **Xie P, Wang G, Li H, Liang J and Gao X** (2020) Circularly polarized Fabry-Perot antenna employing a receiver–transmitter polarization conversion metasurface. *IEEE Transactions on Antennas and Propagation* **68**(4), 3213–3218. doi:10.1109/TAP.2019.2950811

https://doi.org/10.1017/S175907872500011X Published online by Cambridge University Press

9. **Vaidya AR, Gupta RK, Mishra SK and Mukherjee J** (2014) Right-hand/left-hand circularly polarized high-gain antennas using partially reflective surfaces. *IEEE Antennas and Wireless Propagation Letters* **13**, 431–434. doi:10.1109/LAWP.2014.2308926
10. **Xie P and Wang G** (2023) Gain enhancement of circularly polarized Fabry-Perot resonator antenna using simple superstrate[J]. *AEU-International Journal of Electronics and Communications* **165**, 154650.
11. **Lau JY and Hum SV** (2012) A wideband reconfigurable transmitarray element. *IEEE Transactions on Antennas and Propagation* **60**(3), 1303–1311. doi:10.1109/TAP.2011.2180475
12. **Pan W, Huang C, Ma X, Jiang B and Luo X** (2015) A dual linearly polarized transmitarray element with 1-bit phase resolution in X-band. *IEEE Antennas and Wireless Propagation Letters* **14**, 167–170. doi:10.1109/LAWP.2014.2358267
13. **Kaouach H, Dussopt L, Lanteri J, Koleck T and Sauleau R** (2011) Wideband low-loss linear and circular polarization transmit-arrays in V-band. *IEEE Transactions on Antennas and Propagation* **59**(7), 2513–2523. doi:10.1109/TAP.2011.2152331
14. **Baena JD, Glybovski SB, Del Risco JP, Slobozhanyuk AP and Belov PA** (2017) Broadband and thin linear-to-circular polarizers based on self-complementary zigzag metasurfaces. *IEEE Transactions on Antennas and Propagation* **65**(8), 4124–4133. doi:10.1109/TAP.2017.2717964
15. **Diaby F, Clemente A, Pham KT, Sauleau R and Dussopt L** (2018) Circularly polarized transmitarray antennas at Ka-band. *IEEE Antennas and Wireless Propagation Letters* **17**(7), 1204–1208. doi:10.1109/LAWP.2018.2839021
16. **Trentini GV** (1956) Partially reflecting sheet arrays. *IRE Transactions on Antennas and Propagation* **4**(4), 666–671. doi:10.1109/TAP.1956.1144455
17. **Foroozesh A and Shafai L** (2010) Investigation into the effects of the patch-type FSS superstrate on the high-gain cavity resonance antenna design. *IEEE Transactions on Antennas and Propagation* **58**(2), 258–270. doi:10.1109/TAP.2009.2037702
18. **Yang P, Yang R and Li Y** (2021) Dual circularly polarized split beam generation by a metasurface sandwich-based Fabry–Pérot resonator antenna in Ku-band. *IEEE Antennas and Wireless Propagation Letters* **20**(6), 933–937. doi:10.1109/LAWP.2021.3067387
19. **Wang Y and Zhang A** (2021) Dual circularly polarized Fabry–Perot resonator antenna employing a polarization conversion metasurface. *IEEE Access* **9**, 44881–44887. doi:10.1109/ACCESS.2021.3062460
20. **Liu Z-G, Zhang C, Yin R-J and Lu W-B** (2022) Multifunctional low-profile Fabry–Perot resonator antenna integrated with solar cells. *IEEE Transactions on Antennas and Propagation* **70**(8), 7175–7180. doi:10.1109/TAP.2022.3162020

Xin He was born in Dezhou, China, in 1999, and graduated from Jining University in 2022 with a B.S. degree in computer science and technology, and she is currently pursuing a M.S. degree in engineering at Qufu Normal University. Her research interests include Fabry–Perot resonant antenna and multifunctional metasurface.

Wenhua Qin Graduated from the Department of Physics, Qufu Normal University, in1992. Working mainly in the research areas of embedded system applications, Internet of things technology, intelligent information processing, and hadron physics.

Kaize Wang was born in Manzhouli, China, in 1999. He received his bachelor's degree in electronic information engineering from Beijing University of Technology in 2021. He is currently pursuing a master's degree in engineering at Qufu Normal University. His current research interests include 5G millimeter wave magnetoelectric dipole antennas and arrays.

Juan Xu was born in 1982 and graduated from Nanjing University of Science and Technology in 2016 with a Ph.D. in electronic science and technology. She is currently an associate professor of Cyber Science and Engineering, at Qufu Normal University. Her research interests mainly include microwave/millimeter wave circuits and systems, integrated circuits, antenna array optimization and beam forming, multifunctional electromagnetic metasurface, and terahertz biosensing.

https://doi.org/10.1017/S175907872500011X Published online by Cambridge University Press